Volume 2
Number 6
November 2025
Pages 1191-1618

RSC Pharmaceutics

rsc.li/RSCPharma

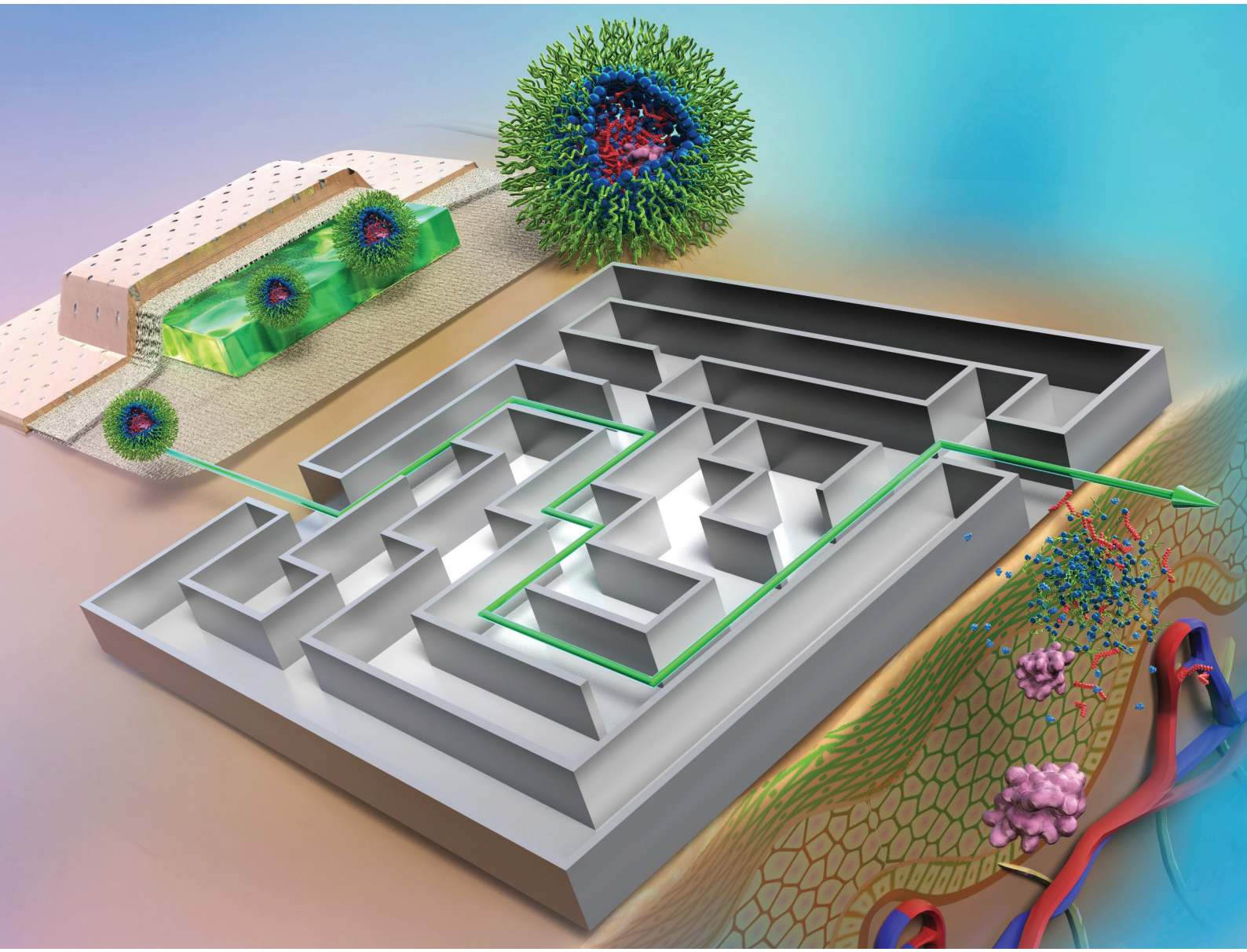

eISSN 2976-8713

ROYAL SOCIETY OF CHEMISTRY

PAPER
Masahiro Goto *et al.*
Needle-free transdermal patches for insulin delivery in diabetes treatment

RSC Pharmaceutics

ROYAL SOCIETY OF CHEMISTRY

PAPER

View Article Online
View Journal | View Issue

Cite this: *RSC Pharm.*, 2025, **2**, 1437

Needle-free transdermal patches for insulin delivery in diabetes treatment†

Yamin Li,[a] Fahmida Habib Nabila,[a] Yoshirou Kawaguchi,[a] Rie Wakabayashi,[a,b,c] Noriho Kamiya[a,b,c] and Masahiro Goto *[a,b,c]

Developing a non-invasive insulin delivery system is crucial for improving diabetes management and patient compliance. Transdermal drug delivery offers a promising alternative to direct injection. However, the strong barrier function of the stratum corneum and the limitations of solution-based formulations hinder the effective penetration of insulin into the skin. To enhance transdermal delivery of insulin, we developed a needle-free ionic liquid-in-oil (IL/O) patch by integrating an IL/O microemulsion with an acrylic pressure-sensitive adhesive. The patch formulation included choline oleate as the biocompatible surface-active IL, sorbitan monolaurate as the co-surfactant, choline propionate as the non-aqueous polar phase, isopropyl myristate as the oil phase, and DURO-TAK® 87-4098 as the adhesive matrix. The IL/O patch adhered stably to the skin and facilitated insulin transport *via* the intercellular route by increasing the fluidity of lipids in the stratum corneum. *In vivo* pharmacodynamics revealed that, compared with the subcutaneous injection (dosage of 10 IU kg^{-1}), the IL/O patch (dosage of 50 IU kg^{-1}) maintained stable blood glucose levels in diabetic mice for up to 72 h, indicating sustained insulin release. The patch demonstrated excellent biocompatibility and low toxicity, making it a promising non-invasive alternative for transdermal insulin delivery and a potential platform for peptide- and protein-based therapeutics.

Received 31st March 2025,
Accepted 4th July 2025

DOI: 10.1039/d5pm00091b

rsc.li/RSCPharma

Introduction

Insulin is a key therapeutic agent for managing type 1 diabetes and advanced type 2 diabetes. Currently, the primary methods of exogenous insulin administration include insulin pens and insulin pumps.[1,2] Insulin pens are used to deliver multiple subcutaneous injections of insulin daily, with each dosage adjusted on the basis of the blood glucose levels (BGLs). However, this method may cause pain, infection, and tissue fibrosis with long-term use, imposing a psychological burden on patients. On the other hand, although insulin pumps offer continuous blood glucose control, they are invasive and technically complex.[3–5] To overcome these limitations, needle-free insulin delivery through oral, intranasal, pulmonary, and transdermal routes has gained significant attention.[6–10] However, the poor permeation of insulin across biological barriers impedes the clinical application of needle-free delivery.[10–12]

Transdermal insulin delivery is a promising non-invasive option that eliminates injection pain and bypasses first-pass metabolism in the gastrointestinal tract, improving drug bioavailability.[13–15] Because transdermal delivery harnesses the body's largest organ—the skin—it has enormous potential for various applications, particularly in skin cancer treatment, gene therapy, pain management, and cardiovascular disease treatment.[16–18] However, the skin, composed of the stratum corneum (SC), epidermis, and dermis, functions as a natural protective barrier. As the outermost layer, the SC is highly hydrophobic and serves as the first line of defense against external substances, making transdermal delivery especially challenging for hydrophilic macromolecular drugs. Owing to its hydrophilicity and relatively large molecular weight (M_w: 5808), insulin exhibits poor transdermal permeation.[10,19,20] To overcome this challenge, microneedles (MNs) have been applied for transdermal insulin delivery. MNs create microchannels in the SC, facilitating drug diffusion into the dermis.[21,22,26] Cui *et al.* developed an MN system with high insulin-loading capacity and glucose-responsive release properties.[22] However, the clinical application of MNs remains challenging[21] owing to issues such as sterility, adjustability, and the safe disposal of sharps waste.[28] Diabetic patients face an increased risk of hospitalization and death from infections

[a]*Department of Applied Chemistry, Graduate School of Engineering, Kyushu University, 744 Motooka, Nishi-ku, Fukuoka 819-0395, Japan*
[b]*Advanced Transdermal Drug Delivery System Center, Kyushu University, 744 Motooka, Nishi-ku, Fukuoka 819-0395, Japan*
[c]*Division of Biotechnology, Center for Future Chemistry, Kyushu University, 744 Motooka, Nishi-ku, Fukuoka 819-0395, Japan*

† Electronic supplementary information (ESI) available. See DOI: https://doi.org/10.1039/d5pm00091b

caused by viruses, bacteria, and fungi.[23] Traditional sterilization methods such as steam autoclaving and dry heating can compromise the integrity of MN patches,[24] impacting both clinical application and large-scale production. Another challenge is the risk of needlestick injuries during post-use handling of MN patches.[25] Because MNs are inconspicuous, MN patches are often improperly disposed in general waste rather than sharps waste, which poses a risk of bloodborne pathogen transmission.

An alternative needle-free system is the transdermal patch, which offers better patient compliance, safety, and simplified post-use handling.[46] A typical transdermal patch consists of three key components: an adhesive matrix, a drug carrier, and a backing layer.[29,30] Among them, pressure-sensitive adhesives (PSAs) are essential, allowing the patch to adhere to the skin with minimal pressure, without requiring heat, solvents, or external activation. In addition to providing adhesion, PSAs serve as a drug carrier matrix, facilitating stable release and prolonged therapeutic effects.[14,31,32] Acrylic-based PSAs are widely used in transdermal formulations owing to their biocompatibility and physicochemical stability.[27] Wang *et al.* developed a transdermal patch based on DURO-TAK® 87-4098 for the treatment of attention-deficit hyperactivity disorder (ADHD).[33] They demonstrated high bioavailability of the patch, highlighting the potential of transdermal patches as a platform for sustained and effective drug delivery.

Ionic liquids (ILs) are liquid salts composed of oppositely charged ions. They remain fluid at temperatures below 100 °C, have a low vapor pressure, and exhibit high thermal stability and excellent solubility, making them widely applicable in biomedicine and pharmaceutical research.[34,35] ILs can serve as efficient solvents for poorly soluble drugs.[36] Additionally, ILs with long hydrophobic tails exhibit surfactant-like properties, classifying them as surface-active ILs. These ILs can self-assemble into various nanostructures, such as micelles, reverse micelles, and vesicles, and have been extensively investigated for applications in transdermal drug delivery systems (TDDS).[37] Choline, a precursor to the neurotransmitter acetylcholine, is a key component of phospholipids in cell membranes and is known for its low toxicity and excellent biocompatibility.[38] Choline-based ILs, synthesized with various organic acids, act as non-aqueous solvents that significantly enhance the solubility of poorly soluble drugs. Choline-based ILs have also been shown to improve the transdermal permeation of both macromolecules and small molecules.[39] For instance, Mitragotri *et al.* demonstrated that a choline geranate (CAGE) IL significantly enhances the transdermal permeation of insulin *in vitro*.[40] In addition, Wu *et al.* reported that both choline citrate and choline geranate significantly improved insulin transdermal delivery and effectively managed blood glucose levels in diabetic rats by permeabilizing the stratum corneum and opening tight junctions.[41] Choline-based ILs function as effective chemical penetration enhancers (CPEs), facilitating transdermal drug delivery.[42,43]

In this study, we developed an IL-in-oil (IL/O) transdermal patch using choline oleate ([Cho][Ole]) as the surfactant, sorbitan monolaurate (Span-20) as the co-surfactant, choline propionate ([Cho][Pro]) as the internal polar phase, isopropyl myristate (IPM) as the continuous oil phase, and DURO-TAK® 87-4098 (DT-4098) as the adhesive. The ILs, CPEs, and PSAs were selected because they exhibit low toxicity and good biocompatibility.[44–47] We performed *in vitro* transdermal permeation tests along with *in vivo* pharmacodynamic and pharmacokinetic evaluations of the developed patch formulation. The results show that the patch exhibits excellent transdermal permeation and can effectively manage blood glucose for 72 hours in diabetic mice, demonstrating strong sustained-release capabilities.

Experimental section

Materials

Insulin, human, recombinant (lot CAM195, potency ≥27.5 units per mg), propionic acid, and fluorescein isothiocyanate isomer I (FITC-I) were procured from Wako Pure Chemical Industries (Osaka, Japan). Choline hydroxide ([Cho][OH]), choline bicarbonate ([Cho][HCO_3]), sorbitan monolaurate (Span-20), and human insulin enzyme-linked immunosorbent assay (ELISA) kits were purchased from Sigma–Aldrich (St. Louis, MO, USA). Oleic acid and IPM were purchased from Tokyo Chemical Industries (Tokyo, Japan). PD-10 Sephadex G-25 M columns were purchased from Sankei Chemical Co. (Kagoshima, Japan). Dulbecco's phosphate-buffered saline (D-PBS) and trypsin/ethylenediaminetetraacetic acid (EDTA) (0.25% trypsin/1 mM ethylenediaminetetraacetic acid) were purchased from Nacalai Tesque (Kyoto, Japan). Methanol (MeOH) and acetonitrile (ACN) were obtained from Fujifilm Wako Pure Chemical Corporation (Osaka, Japan). DURO-TAK® 87-4098 was a gift from Henkel Corporation (Minoh, Japan).

The other chemicals and solvents were of analytical grade and used without further purification.

Animals

Yucatan micropig (YMP) skin was received from Charles River Japan (Yokohama, Japan) and stored in the frozen state at −80 °C.

Male BKS.Cg-m+/+ Lepr^{db} mice (6 weeks old) and male BALB/c mice were purchased from Kyudo (Saga, Japan) and nurtured under natural conditions for 1 week prior to the experiments. All animal experiments were approved by the Ethics Committee for Animal Experimentation of Kyushu University (No. A22-231-0 and A24-173-0) and carried out following the guidelines set by the Science Council of Japan.

Insulin in the IL and circular dichroism (CD) spectroscopy

Insulin was dissolved in PBS or [Cho][Pro]. [Cho][Pro] was synthesized and its structure confirmed following established protocols.[44,48] For the detailed reaction formula, refer to Fig. S1.† The water content of the IL was adjusted to approximately 13 wt%, and the final water content was confirmed

using a Karl Fischer moisture meter (KF titration, CA-310, Nittoseiko Analytech, Yamato, Japan).

The solubility of insulin in [Cho][Pro] was visually confirmed through the formation of a clear solution. [Cho][Pro] in the transparent aqueous solution was removed using a dialysis membrane with a molecular weight cut-off (MWCO) of 3.5 kDa. Dialysis proceeded for 24 hours at room temperature with 1× PBS as the dialysate. Fresh insulin dissolved in PBS was used as the control. CD spectroscopy was performed using a J-1500 CD spectrometer (JASCO, Tokyo, Japan) under the conditions specified in Table 1.

Preparation and characterization of IL/O MEs

The surface-active IL [Cho][Ole] was synthesized following a previously reported protocol,[47,48] and its structure was characterized using ^{1}H NMR spectroscopy. The IL/O ME was prepared following a previously established protocol.[49] A predetermined amount of insulin was dissolved in 2.5% (w/w) [Cho][Pro]. Then, a clear solution was prepared by dissolving 7.5% (w/w) [Cho][Ole] and 5.0% (w/w) Span-20 in 85% (w/w) IPM with stirring. The IL/O ME (3 mg mL^{-1}) containing insulin was formulated by incorporating the polar phase, [Cho][Pro], into the oil phase (Fig. S2†), as detailed in Table S1.† The average hydrodynamic radius (R_H) of the particles was determined by dynamic light scattering (DLS) using a Zetasizer Nano ZSP system (Malvern Panalytical, Malvern, UK). The sample was added to a glass cuvette, and the temperature was maintained at 25 ± 0.1 °C during the measurements. Each sample was measured 10 times, and the values were analyzed using Zetasizer 7.03. Additionally, the IL/O ME containing [Cho][Ole] (ME-[Cho][Ole]) was stored at room temperature for 50 days, and its stability was confirmed by reevaluating the particle size using DLS.

Preparation of IL/O transdermal patches

IL/O patches were prepared using an established solvent evaporation protocol.[48] DURO-TAK® 87-4098 (DT-4098) was mixed with ME-[Cho][Ole] in a 1 : 1 weight ratio. The mixture was stirred with a vortex mixer until homogeneous to form the base. The mixture was deposited onto a polyethylene terephthalate (PET) release liner and uniformly spread *via* a K-control coater (RK Prints, UK) to ensure consistent thickness. The organic solvent in the patch was subsequently removed by drying at 60 °C for 20 min in a vacuum drying oven (Ishii Laboratory Works Co., Osaka, Japan). A support made of PET was then affixed to the base material, which was shielded from light and allowed to air-dry overnight at room temperature (Scheme 1).

Table 1 Parameters for CD measurements[a]

Cell	Path length (cm)	Wavelength range (nm)	Integral count	Temperature (°C)
Quartz cell	0.1	190–260	4	25

[a] CD spectral data were processed using an adaptive smoothing algorithm to minimize noise interference.

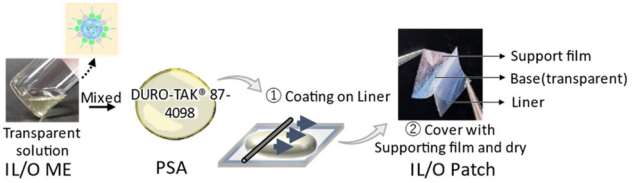

Scheme 1 Schematic illustration of the preparation of the IL/O patch.

Calculation of the drug content of IL/O patches

After cleaning with 99% ethanol and drying, the peeled IL/O patch liner was weighed $\boldsymbol{Y}$ [mg]. Subsequently, the weight $\boldsymbol{X}$ [mg] of the support material alone was measured. The cut area $\boldsymbol{Z}$ [cm^2] of the IL/O patch was calculated using eqn (1), with the surface density of the support of 2.83 mg cm^{-2}. The weight per unit area $\boldsymbol{V}$ [mg cm^{-2}] of the IL/O patch was then calculated using eqn (2). The amount of IL/O solution per unit area (original solution amount) $\boldsymbol{W}$ [mg cm^{-2}] was determined using eqn (3), with the weight ratio of the IL/O solution to DT-4098 in the dried IL/O patch of 1 : 0.4. The amount of insulin per unit area [μg cm^{-2}] was calculated using eqn (4), with the weight ratio of insulin, internal phase, surfactant, co-surfactant, and oil in the IL/O solution of 3 : 25 : 75 : 50 : 850.

$$\text{Cutting area } \boldsymbol{Z}\ [\text{cm}^2] = \frac{X\ [\text{mg}]}{\text{areal density of supportment } (2.83 mg\ cm^{-2})} \quad (1)$$

$$\text{Weight of IL/O patch } \boldsymbol{V} \text{ per unit area } [\text{mg cm}^{-2}] = \frac{(Y - X)\ \text{mg}}{(Z\ [cm^{-2}])} \quad (2)$$

$$\text{IL/O solution volume } \boldsymbol{W} \text{ per unit area } [\text{mg cm}^{-2}] = \frac{V\ [\text{mg cm}^{-2}]}{1 + 0.4} \quad (3)$$

$$\text{Amount of insulin per unit area } [\mu\text{g cm}^{-2}] = \frac{3 \times 1000 \times W\ [\mu\text{g cm}^{-2}]}{3 + 25 + 75 + 50 + 850} \quad (4)$$

In vitro YMP skin permeation and CLSM observations

YMP skin (The Jackson Laboratory, USA) was employed to evaluate *in vitro* transdermal permeation as described previously.[50,51] In brief, the patch or solution formulation was applied to the YMP skin in a vertical Franz cell. The ME formulation or FITC–insulin-loaded IL/O patch (1.5 × 1.5 cm) was placed in the donor compartment. PBS and a stirrer were added to the receiver compartment of the vertical Franz cell. Incubation proceeded for 12, 24, 36, and 48 h at 32.5 °C with continuous stirring in a thermostatic reactor. After incubation, the YMP skin was removed from the Franz cell, and any remaining patch was removed using Kimwipes soaked in 20% ethanol. The skin was then cut and divided into 16 equal sec-

tions using a scalpel. FITC–insulin was extracted from the skin using an extraction solution composed of PBS, ACN, and MeOH in a 2 : 1 : 1 ratio. Extraction proceeded overnight with continuous shaking to ensure efficient recovery. The amount of FITC–insulin in the skin was quantified using a microplate reader.

To evaluate the profile of insulin permeation through the YMP patch, post-incubation skin specimens were cryopreserved and sectioned. Following incubation, the skin samples were bisected and embedded in an optimized matrix medium (Sakura Finetek, Tokyo, Japan) prior to flash-freezing at −80 °C. The samples were cryosectioned using a precision cryostat microtome (CM1860UV, Leica Biosystems, Wetzlar, Germany) to obtain transverse sections (20 μm thick), which were immediately mounted onto glass slides. Fluorescence patterns within the cutaneous layers were subsequently analyzed using high-resolution confocal laser scanning microscopy (CLSM; LSM900, Carl Zeiss, Jena, Germany).

Patch-induced structural changes in the SC layer

The effect of the patch on the SC layer was determined using Fourier-transform infrared (FT-IR) spectroscopy. The SC layer and molecular interactions were characterized using literature protocols with optimized parameters.[15,52] To prepare SC sheets, YMP skin specimens were oriented with the SC layer facing downward, wrapped in aluminum foil, and thermally equilibrated at 60 °C for 10 min in an aluminum block incubator. The epidermal layer was subsequently separated using fine-tip tweezers, inverted (epidermal side down), and enzymatically digested in trypsin-EDTA solution (0.25% trypsin, 1 mM EDTA·4Na) for 24 h. Post-digestion, the solution was decanted, and the samples were rigorously rinsed with Milli-Q water, followed by complete air-drying. The dried epidermal sheets were sectioned into 1 cm^2 fragments for subsequent analysis. Structural alterations in patch-treated SC sheets were evaluated using FTIR spectroscopy (Spectrum Two, PerkinElmer, Waltham, MA, USA), with untreated SC sheets serving as negative controls.

Transdermal permeation pathway of insulin

FITC-loaded patches were administered to the auricular region of BALB/c mice and maintained for 6 hours post-application. After euthanasia, the treated ears were surgically excised, and the ear surfaces were decontaminated using 20% ethanol to completely remove patch residues. Specimens were then mounted on glass slides with ProLong™ Glass Antifade Mountant (Thermo Fisher Scientific, Waltham, MA, USA) and coverslipped for stabilization. SC permeation profiles were observed using confocal laser scanning microscopy (CLSM; LSM900, Carl Zeiss, Jena, Germany). *Z*-stacks were acquired to resolve three-dimensional fluorescence patterns.

In vivo pharmacodynamics in BKS diabetic mice

In vivo pharmacodynamics in BKS.Cg-m+/+Leprdb mice was investigated using previously reported methods with slight modifications.[15,49] Mice (n = 5 per group) were acclimatized for 7 days under standard housing conditions with *ad libitum* access to food and water. Prior to the experiment, dorsal hair was removed. To evaluate glucose homeostasis, three cohorts were established: (1) non-treated control, (2) insulin subcutaneous injection, and (3) IL/O transdermal patch incorporating surface-active [Cho][Ole] (P-[Cho][Ole]). In the injection group, insulin was dissolved in Dulbecco's phosphate-buffered saline (D-PBS) and administered at a dosage of 10 IU kg^{-1} body weight. In the transdermal patch group, a 50 IU kg^{-1} dose was applied to the depilated dorsal skin and secured with an occlusive dressing for controlled delivery. BGLs were measured at various time points post-administration, and therapeutic efficacy was evaluated by comparing the attenuation of hyperglycemic excursions across the groups.

In vivo pharmacokinetics

In vivo pharmacokinetics in BALB/c mice was investigated by measuring the plasma insulin concentration using previously reported methods.[49] Six-week-old BALB/c mice (n = 5 per group) were randomized into three cohorts: (1) non-treated control, (2) subcutaneous injection of insulin in D-PBS (dosage of 10 IU kg^{-1}), and (3) transdermal delivery of insulin-loaded P-[Cho][Ole] (dosage of 50 IU kg^{-1}). In the injection group, mice were subcutaneously administered insulin. In the patch group, patches were applied to the depilated dorsal skin following pharmacodynamic protocols. Blood samples were collected in heparinized tubes at predetermined intervals post-administration. Plasma was isolated by centrifugation (1200 rpm, 15 min, 4 °C), and the plasma insulin concentration was determined using a human insulin ELISA kit. Transdermal patches were removed 24 hours post-application to terminate drug administration.

In vivo biocompatibility of insulin patches

The test patch was applied to the dorsal skin of mice following pharmacodynamic protocols. Patches were left in place for a 24-hour administration period before removal. In the positive control group, mice were subcutaneously injected with insulin (dosage of 10 IU kg^{-1}). The body mass was measured and recorded daily throughout a 10-day observational phase to assess systemic physiological impacts.

Statistical analysis

Statistical analyses were conducted using Microsoft Excel 2019 (Microsoft, Redmond, DC, USA), with p-values calculated *via* Student's t-tests. Significance is indicated as $*p < 0.05$, $**p < 0.01$, $***p < 0.001$, and $****p < 0.0001$. Data are presented as the mean ± standard error, unless otherwise specified.

Results and discussion

Structural stability of insulin in [Cho][Pro]

Human insulin, a 51-amino acid protein hormone featuring two α-helical domains, mediates glucose homeostasis through specific interactions with transmembrane insulin receptors.[53]

Its hydrophobicity poses significant challenges for transdermal delivery. In this study, the solubility of insulin in [Cho][Pro] with different water contents was evaluated (Fig. S4†). Insulin was introduced into [Cho][Pro] containing 6 (initial), 15, and 20 wt% water. Visual inspection revealed that all solutions remained clear and transparent even after 24 hours at room temperature, with no visible precipitation. CD spectroscopy was performed to assess formulation-induced conformational changes. The CD spectrum of insulin dissolved in [Cho][Pro] containing 15 wt% water showed characteristic α-helical signatures: two distinct minima at 210 and 225 nm, matching the spectrum of insulin in fresh PBS, the control (Fig. 1).[54] These findings indicate that insulin retains its native structure in [Cho][Pro].

Preparation of IL/O patches

To fabricate IL/O patches, a stable IL/O ME formulation containing nanoparticles was first prepared. The IL/O ME was formulated with the following components: [Cho][Pro], the polar phase, served as a structural stabilizer to maintain insulin's native conformation; [Cho][Ole], the surface-active IL, was added to enhance transdermal permeation *via* SC lipid fluidization; Span-20 (HLB = 4.3), the co-surfactant, was included to synergistically improve system stability and enhance penetration; and IPM, the biocompatible oil phase. IL/O MEs were prepared using [Cho][Pro] with different water contents. DLS analysis revealed that using [Cho][Pro] with approximately 15 wt% water produced nanoparticles of approximately 20 nm, which were stable for at least 50 days at room temperature (Fig. S5a, b and Table S2†). However, using [Cho][Pro] with lower water content led to the formation of larger nanoparticles (size >90 nm) with poor uniformity (PDI >0.3) (Fig. S5c and Table S3†). In contrast, [Cho][Pro] with higher water content failed to form nanoparticles, resulting in a turbid solution. This suggests that insufficient polarity of the internal aqueous phase weakens interactions between [Cho][Pro] and the surfactant's hydrophilic heads, leading to larger, less uniform nanoparticles. Conversely, excessive polarity of the internal phase hinders its encapsulation within the nanoparticle core, causing phase separation and turbidity. Therefore, optimizing the water content to achieve the appropriate polarity of the internal phase is crucial for enhancing the stability of both the IL/O solution and the resulting nanoparticles. Previous studies have demonstrated that IL/O MEs exhibit enhanced transdermal permeation, attributed to their nanoscale particle size (<20 nm) and the interactions between the surface-active ILs and skin. However, the liquid nature of these formulations poses challenges in maintaining skin adhesion and achieving precise dose administration, and under the same dosing conditions, the ME formulation exhibits limited sustained release. To achieve long-term stability of the BGLs, improving the transdermal penetration efficiency of the formulation is crucial. This can be achieved by incorporating PSAs into transdermal patch systems. Integrating acrylic-based PSAs not only improves skin adhesion but also enhances the penetration efficiency.

IL/O ME-based patches were fabricated by integrating the IL/O ME formulation with DT-4098 PSA. Details of DT-4098 are summarized in Table S4.† DT-4098 was selected because of its superior adhesion properties and biocompatibility. Owing to the specific structural characteristics of the polymer matrix, the nanoparticles were effectively incorporated into the acrylic polymer network. The IL/O patch exhibited higher viscoelasticity compared to the 8% HEC gel, demonstrating a softer texture than the blank DT-4098 patch, indicating its potential for practical application. Additionally, the rheological properties confirmed the solid characteristics of the IL/O patch, supporting its adhesive performance. Previous studies have shown that transdermal penetration is closely linked to patch thickness, with 100 μm-thick patches yielding optimal results.[48] Thus, 100 μm-thick patches were used in all subsequent experiments.

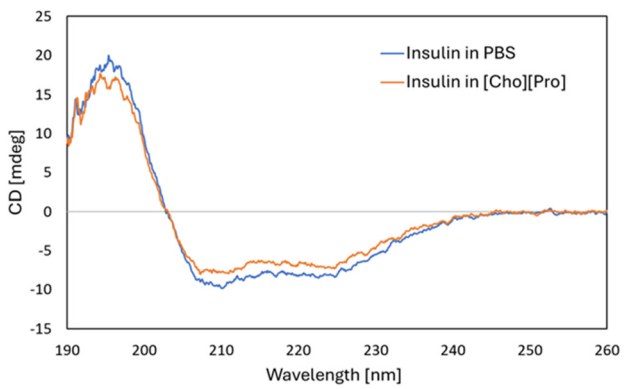

Fig. 1 CD spectral analysis of insulin under ambient conditions confirmed the preservation of its secondary structure integrity in the aqueous microenvironment.

In vitro skin penetration

The *in vitro* skin penetration of P-[Cho][Ole] and ME-[Cho][Ole] was evaluated using YMP skin as the model skin. The amount of FITC–insulin that permeated through the skin (permeation) and into the skin (penetration) was quantified using a plate reader. The permeation percentage was then calculated relative to the administered amount. After 48 hours of incubation, only a small amount of FITC–insulin was detected in PBS-treated skin, whereas a significantly high amount of insulin was detected in skin treated with either P-[Cho][Ole] or ME-[Cho][Ole]. The amount of insulin penetrating the skin from each formulation is presented in Fig. S6.† Because the donor area was fixed at 0.785cm^2, the administered amount (Table S5†) differed between the patch and ME formulations. Therefore, the penetration percentage was used to assess the penetration efficiency across different formulations. The penetration and permeation percentages of ME-[Cho][Ole] were 2.79 ± 0.23% and 0.22 ± 0.15%, respectively, while those of P-[Cho][Ole] were 6.50 ± 0.45% and 0.14 ± 0.023%, respectively. Compared to ME-[Cho][Ole], P-[Cho][Ole] exhibited a 2.58-fold higher transdermal delivery ratio (Fig. 2a). The release of

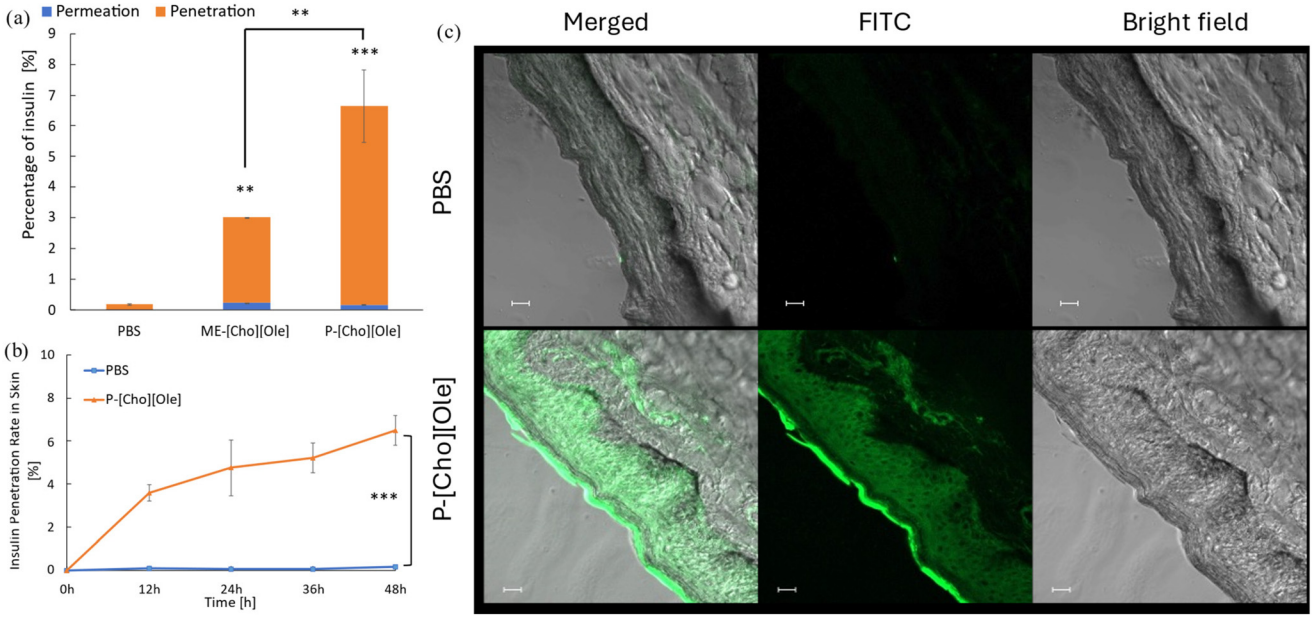

Fig. 2 *In vitro* permeation of insulin through YMP skin. (a) Total permeated insulin (%) at 48 h. (b) Time-dependent FITC–insulin permeation profiles. (c) CLSM images of YMP skin treated with a FITC–insulin patch for 48 h (20× lens, scale bar: 20 μm). n = 3, mean ± SD, $^{**}p < 0.01$, and $^{***}p < 0.001$. Statistical significance compared with PBS using Tukey's *post hoc* test.

insulin from P-[Cho][Ole] gradually increased over time. After 12 h, the penetration percentage of the patch group was significantly higher than that of the PBS group (Fig. 2b). These results indicate that P-[Cho][Ole] can significantly enhance the transdermal delivery of insulin. Furthermore, CLSM images of skin cross-sections (Fig. 2c) confirmed that the patch facilitated insulin delivery into the SC and deeper layers of the skin.

As a hydrophilic macromolecule (M_w: 5808), insulin encounters 2 major transdermal barriers that hinder its passive diffusion: the hydrophobic and densely packed structure of the SC. Consequently, the PBS group did not exhibit significant skin permeation. In the IL/O ME formulation, insulin is solubilized in the polar phase [Cho][Pro], while the surface-active IL [Cho][Ole] interacts with stratum corneum (SC) lipids, disrupting the barrier function and enhancing transdermal delivery. The double bonds in the unsaturated fatty acid moiety of [Cho][Ole] induce bending and disorder in lipid structures, further promoting skin permeability.[49] Isopropyl myristate (IPM), a well-established permeation enhancer, integrates into the SC lipid bilayers to increase drug solubility and facilitate diffusion. When combined with PSA, IPM improves the mobility of PSA chains, functioning as a plasticizer to further enhance drug release.[55–57] In the patch system, the network structure of DT-4098 enables uniform nanoparticle dispersion, thereby enhancing transdermal absorption. Additionally, the IPM/PSA mixture strengthens skin adhesion, reduces moisture loss, and increases SC hydration, which cause corneocyte swelling and open wider, more efficient pathways for drug penetration.[58] Therefore, the patch formulation not only promotes insulin release but also enhances PSA mobility through its interaction with the IL/O ME system, thereby further improving transdermal delivery efficiency.

Skin permeation mechanism

The SC plays a crucial role in the skin's barrier function, regulating transdermal drug permeation. Drug permeation through skin primarily occurs *via* three pathways: intercellular, intracellular, and transfollicular routes.[59,60] To investigate the permeation pathways, BALB/c mouse ears were treated with FITC-insulin loaded PBS and P-[Cho][Ole]. After 6 h of incubation, the formulations were removed, and the mice were euthanized. The ears were then collected, and the permeation pathways were observed using CLSM, as shown in Fig. 3a. Fluorescence was primarily observed along the edges of corneocytes, indicating that the predominant permeation pathway was the intercellular route. Previous studies have reported that [Cho][Ole] and IPM enhance lipid fluidity through strong interactions with intercellular lipids.[49,61,62]

FTIR spectroscopy was employed to elucidate the permeation mechanism. The intercellular lipid lamellae of the SC are primarily composed of ceramides (CERs), free fatty acids, and cholesterol. Free fatty acids consist of saturated and α-hydroxy carbon chains, and the properties of these lipids are closely related to the SC barrier function.[63] Therefore, FTIR spectra were acquired to analyze the structural arrangement of alkyl chains in SC sheets treated with P-[Cho][Ole]. As shown in Fig. 3b and c, the peaks at 2850 cm^{-1} and 2920 cm^{-1} in the spectrum of P-[Cho][Ole]-treated SC sheets exhibited a blue shift relative to those in the spectrum of PBS-treated SC sheets. These peaks correspond to the symmetric and asymmetric stretching vibrations of CH_2 groups (Fig. 3d and e). These

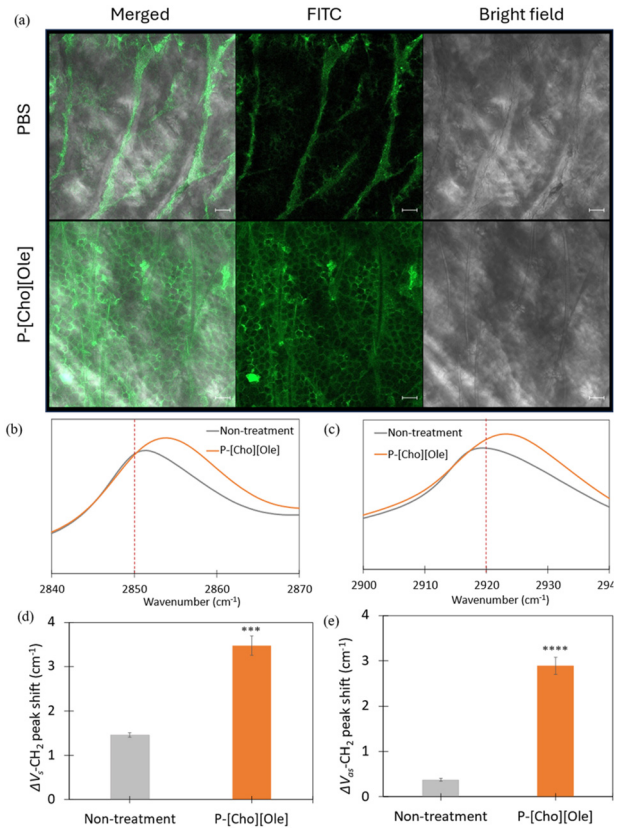

Fig. 3 Skin permeation mechanism. (a) CLSM images of the SC treated with PBS or P-[Cho][Ole]. (b and c) FTIR spectra of the SC from P-[Cho][Ole] treated or untreated YMP. FTIR peaks around 2850 and 2920 cm^{-1} correspond to CH_2 symmetric and asymmetric vibrational modes of SC lipids. (d and e) Shift in CH_2 vibrational peaks relative to theoretical values (10× lens, scale bar: 50 μm). n = 3, mean ± SD, ***p < 0.001, and ****p < 0.0001. Statistical significance compared with non-treated samples using Tukey's *post hoc* test.

shifts reveal an increase in the ratio of *gauche*/*trans* conformers, and because the *gauche* conformation leads to chain kinks, a higher proportion of *gauche* conformers indicates a more fluid SC structure and a compromised barrier function.[64,65] Owing to its intrinsic properties, the IL can diffuse into SC lipid layers and weaken intermolecular interactions among lipids.[66] Furthermore, the combined effects of Span-20, [Cho][Ole], and IPM in the ME formulation significantly enhance the fluidity of SC, further improving permeability.

In vivo pharmacodynamics and BGL reduction in BKS diabetic mice

The effect of P-[Cho][Ole] on the BGLs of BKS.Cg-m+/+Lepr^{db} diabetic model mice was assessed (Fig. 4a). Untreated diabetic mice served as the negative control, while mice receiving a subcutaneous injection of 100 μL of insulin-loaded D-PBS (dosage of 10 IU kg^{-1}) were designated as the positive control. The P-[Cho][Ole] treatment group received insulin-loaded P-[Cho][Ole] at a dosage of 50 IU kg^{-1}, while the ME-[Cho][Ole] group was treated with an insulin-loaded IL/O ME solution formulation, also at a dosage of 50 IU kg^{-1}. Non-treated mice consistently remained in a hyperglycemic state throughout the experiment. In contrast, mice receiving the subcutaneous injection exhibited a rapid and significant 72% reduction in their BGLs within 1 hour of injection and then an increase in their BGLs, into the hyperglycemic range, after 3 h of injection. In the ME-[Cho][Ole] group, a decrease in BGLs was observed, which remained within the normal range for 24 hours, with a maximum reduction of around 29% at 12 hours. In contrast, in the P-[Cho][Ole] treatment group, BGLs gradually decreased post-administration and remained within the normal range for over 48 hours, with a maximum reduction of 32% at 12 hours (Fig. 4b and c). Notably, the release duration of P-[Cho][Ole] was longer than that of ME-[Cho][Ole], indicating the sustained-release effect of the patch formulation (Fig. 4b). The BGL-lowering effect of P-[Cho][Ole] arises from the enhanced insulin delivery, which is attributed to the IL, Span-20, and IPM interacting with skin lipids to disrupt the surface barrier. Additionally, DT-4098, with its mesh-like structure, may enable the gradual release of nanoparticles, facilitate slow transdermal drug delivery and effectively maintain long-term BGL stability.[67]

In vivo pharmacokinetics

The efficiency of transferring insulin from the transdermal patch to blood was evaluated using non-diabetic BALB/c mice as model animals. Mice receiving subcutaneous injections of insulin-loaded D-PBS (dosage of 10 IU kg^{-1}) served as the positive control, while non-treated mice were the negative control. Mice treated with P-[Cho][Ole] received a dose of 50 IU kg^{-1}. Blood samples were collected at various time points, and the plasma insulin concentration was determined using an insulin ELISA kit. The plasma insulin concentration–time profile following transdermal administration is presented in Fig. 5b. As shown in Fig. 5b, in the subcutaneous injection group, the plasma insulin concentration rapidly increased within 1 h and returned to the baseline levels by 3 h. In the P-[Cho][Ole] group, the plasma insulin concentration gradually increased, peaking at 12 h before returning to the normal level by 48 h. This trend aligns with the observed pharmacodynamic response. Insulin released from the patch may initially accumulate in the SC and gradually permeate through the skin, maintaining its concentration in blood over an extended period.

Evaluation of patch biocompatibility

The biocompatibility of P-[Cho][Ole] was evaluated with an *in vitro* skin irritation experiment using LabCyte EPI Model-24, as reported previously. The results revealed that the patch did not induce significant irritation.[48] Biocompatibility was also assessed by monitoring the body mass of BALB/c mice. Specifically, P-[Cho][Ole] was applied to BALB/c mice, the patch was removed after 24 hours, and the body mass was measured over a 10-day period. As shown in Fig. 6, the body mass of P-[Cho][Ole]-treated mice was not significantly different from that of non-treated mice, confirming the biocompatibility of P-[Cho][Ole].

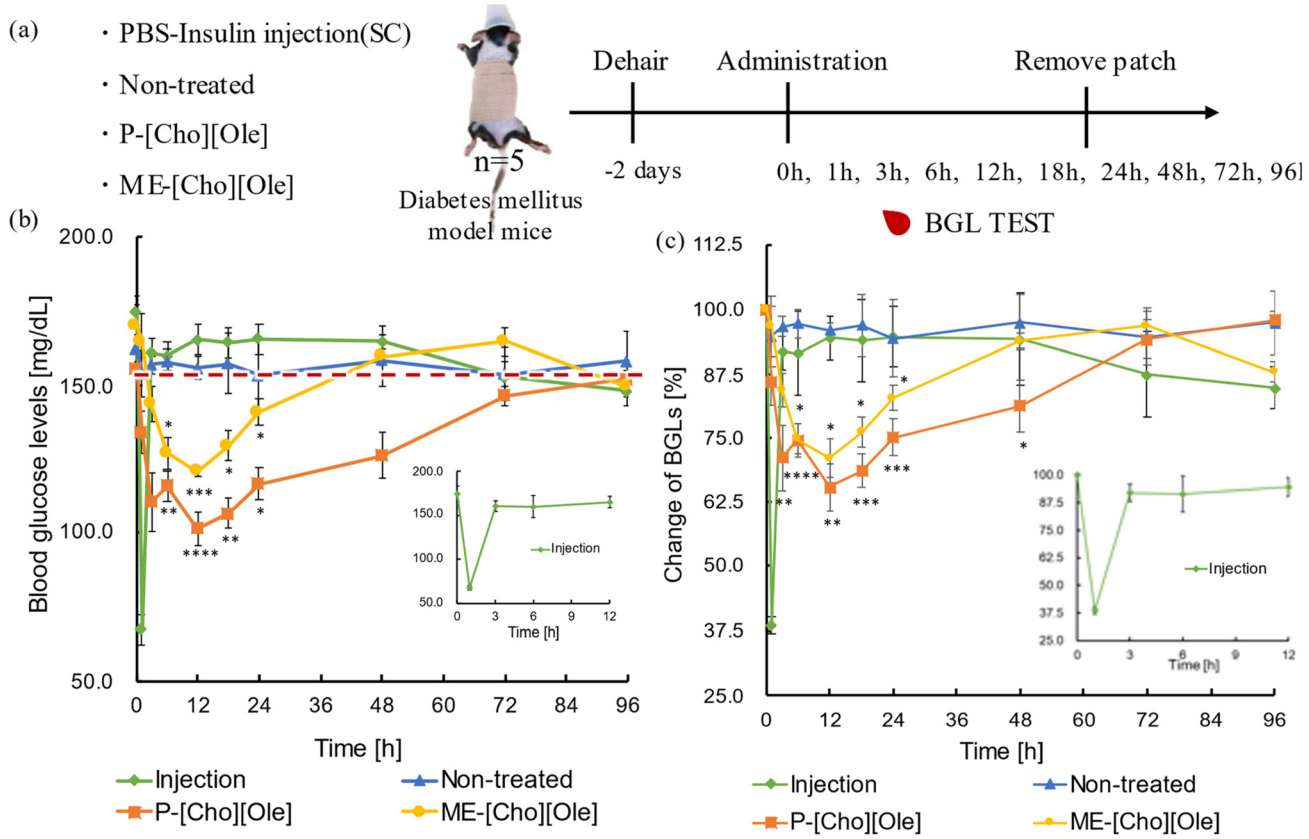

Fig. 4 Impact of transdermal patch on blood glucose levels (BGL). (a) Timeline of this experiment. (b) Changes in the BGL of diabetic mice over time. (c) Comparison of BGL reduction by different patches relative to baseline values. n = 5, mean ± SD, *p < 0.05, **p < 0.01, ***p < 0.001, and ****p < 0.0001. Statistical significance compared with non-treated samples using Tukey's *post hoc* test.

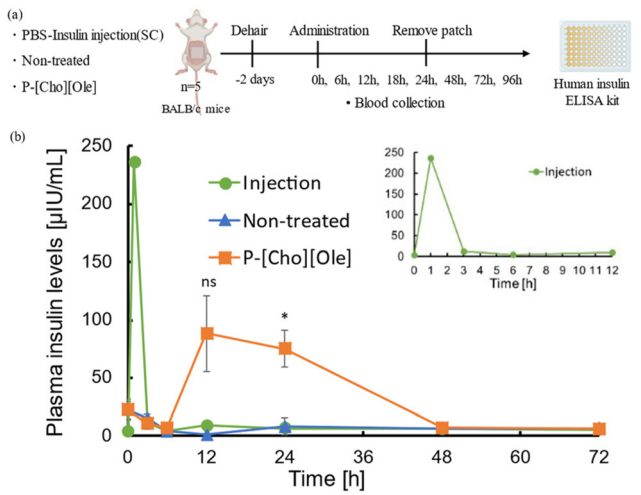

Fig. 5 Bioavailability of insulin from transdermal patches in BALB/c mice. (a) Experimental timeline. (b) Plasma concentration–time profiles after administration. n = 5, mean ± SD, ns, not significant, and *p < 0.05. Statistical significance compared with non-treated samples using Tukey's *post hoc* test.

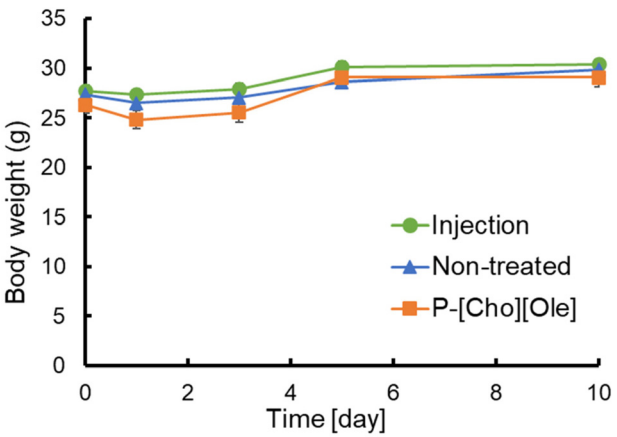

Fig. 6 Systemic biocompatibility of the patch was assessed by continuously monitoring the body mass of treated and non-treated BALB/c mice.

Conclusions

In the present study, we successfully developed an IL/O ME-based transdermal patch using biocompatible [Cho][Ole] as the IL/O phase and DT-4098 as the adhesive. Insulin main-

tained its native structure within the internal polar phase of the patch, ensuring its stability and bioactivity. Compared with conventional PBS and IL/O ME formulations, P-[Cho][Ole] exhibited significantly enhanced skin penetration, particularly into YMP skin. P-[Cho][Ole] permeated through the intercellular pathway of the SC, interacting with intercellular lipids to increase their fluidity, thereby improving insulin's transdermal permeation.

In vivo pharmacodynamics revealed that P-[Cho][Ole] effectively maintained the BGLs within the normal range for over 72 hours, indicating the sustained release of insulin. Notably, insulin delivered *via* P-[Cho][Ole] remained in circulation longer than insulin delivered *via* subcutaneous injection, suggesting a prolonged therapeutic effect. Owing to its stability, biocompatibility, and convenience, P-[Cho][Ole] (with DT-4098 as the adhesive) is a promising transdermal carrier for protein and peptide drugs. Its enhanced skin permeation and sustained-release properties make it a promising alternative to conventional injection formulations, offering a non-invasive and patient-friendly approach for the treatment of chronic diseases requiring frequent drug administration.

Author contributions

Y. L.: writing of the original draft, investigation, and methodology. F. H. N.: investigation and editing. R. W. and Y. K.: investigation and methodology. N. K.: methodology, validation, and writing – reviewing, and editing. M. G.: conceptualization, supervision, validation, and editing. All authors contributed to the discussion of the paper and approved the manuscript.

Conflicts of interest

There are no conflicts to declare.

Data availability

The data supporting this article have been included as part of the ESI.†

Acknowledgements

The authors acknowledge financial support from the Japan Society for the Promotion of Science (KAKENHI numbers JP22K18314 and JP24KJ1798) and AMED (22ak0101174h0002). We thank Edanz (https://jp.edanz.com/ac) for editing a draft of this manuscript.

References

1 Y. Zhang, J. Yu, A. R. Kahkoska, J. Wang, J. B. Buse and Z. Gu, *Adv. Drug Delivery Rev.*, 2019, **139**, 51–70.
2 L. M. Wilson and J. R. Castle, *Diabetes Technol. Ther.*, 2020, **22**(12), 929–936.
3 J. L. Selam, *J. Diabetes Sci. Technol.*, 2010, **4**(3), 505–513.
4 J. Pickup and H. Keen, *Diabetes Care*, 2002, **25**(3), 593–598.
5 C. Berget, L. H. Messer and G. P. Forlenza, *Diabetes Spectrum*, 2019, **32**(3), 194–204.
6 N. Easa, R. G. Alany, M. Carew and A. Vangala, *Drug Discovery Today*, 2019, **24**(2), 440–451.
7 N. J. Hunt, G. P. Lockwood, S. J. Heffernan, J. Daymond, M. Ngu, R. K. Narayanan, L. J. Westwood, B. Mohanty, L. Esser, C. C. Williams, Z. Kuncic, P. A. G. McCourt, D. G. Le Couteur and V. C. Cogger, *Nat. Nanotechnol.*, 2024, **19**(4), 534–544.
8 M. Hallschmid, *J. Neuroendocrinol.*, 2021, **33**(4), e12934.
9 T. K. Mandal, *Am. J. Health-Syst. Pharm.*, 2005, **62**(13), 1359–1364.
10 H. Li, Y. Shi, X. Ding, C. Zhen, G. Lin, F. Wang, B. Tang and X. Li, *Int. J. Biol. Macromol.*, 2024, **274**(Pt 2), 133452.
11 E. S. Khafagy, M. Morishita, Y. Onuki and K. Takayama, *Adv. Drug Delivery Rev.*, 2007, **59**(15), 1521–1546.
12 F. Sabbagh, I. I. Muhamad, R. Niazmand, P. K. Dikshit and B. S. Kim, *Int. J. Biol. Macromol.*, 2022, **203**, 222–243.
13 W. Y. Jeong, M. Kwon, H. E. Choi and K. S. Kim, *Biomater. Res.*, 2021, **25**(1), 24.
14 T. Karve, A. Dandekar, V. Agrahari, M. M. Peet, A. K. Banga and G. F. Doncel, *Adv. Drug Delivery Rev.*, 2024, **210**, 115326.
15 F. H. Nabila, R. Islam, L. Yamin, K. Yoshirou, R. Wakabayashi, N. Kamiya, M. Moniruzzaman and M. Goto, *ACS Biomater. Sci. Eng.*, 2025, **11**(1), 402–414.
16 W. Zhu, T. Wei, Y. Xu, Q. Jin, Y. Chao, J. Lu, J. Xu, J. Zhu, X. Yan, M. Chen, Q. Chen and Z. Liu, *Nat. Commun.*, 2024, **15**(1), 820.
17 P. Singh, I. Muhammad, N. E. Nelson, K. T. M. Tran, T. Vinikoor, M. T. Chorsi, E. D'Orio and T. D. Nguyen, *Drug Delivery Transl. Res.*, 2022, **12**(11), 2613–2633.
18 M. C. Peña-Juárez, O. R. Guadarrama-Escobar and J. J. Escobar-Chávez, *J. Pharm. Innovation*, 2022, **17**(2), 319–332.
19 F. H. Nabila, R. Islam, I. M. Shimul, M. Moniruzzaman, R. Wakabayashi, N. Kamiya and M. Goto, *Chem. Commun.*, 2024, **60**(30), 4036–4039.
20 L. W. Limenh, N. K. Worku, M. Melese, D. Esubalew, E. T. Fenta, M. Hailu, A. Abie, M. G. Mehari, T. E. Dagnaw and A. M. Delie, *Diabetol. Metab. Syndr.*, 2024, **16**(1), 197.
21 J. Zhao, G. Xu, X. Yao, H. Zhou, B. Lyu, S. Pei and P. Wen, *Drug Delivery Transl. Res.*, 2022, **12**(10), 2403–2427.
22 Y. Liu, L. Yang and Y. Cui, *Microsyst. Nanoeng.*, 2024, **10**(1), 112.
23 S. Erener, *Mol. Metab.*, 2020, **39**, 101044.
24 M. T. McCrudden, A. Z. Alkilani, A. J. Courtenay, C. M. McCrudden, B. McCloskey, C. Walker, N. Alshraiedeh, R. E. Lutton, B. F. Gilmore, A. D. Woolfson and R. F. Donnelly, *Drug Delivery Transl. Res.*, 2015, **5**(1), 3–14.
25 A. McConville, C. Hegarty and J. Davis, *Medicines*, 2018, **5**(2), 50.
26 S. Wang, C. Yang, W. Zhang, S. Zhao, J. You, R. Cai, H. Wang, Y. Bao, Y. Zhang, J. Zhang, K. Ji, Y. Zhang, X. Ye, Z. Gu and J. Yu, *ACS Nano*, 2024, **18**(38), 26056–26065.

27 M. A. Droesbeke, R. Aksakal, A. Simula, J. M. Asua and F. E. Du Prez, *Prog. Polym. Sci.*, 2021, **117**, 101396.
28 F. Smith, A. H. Sabri, M. Heppel, I. Fonseca, F. Chowdhury, K. Cheung, S. Willmor, F. Rawson and M. Marlow, *Int. J. Pharm.*, 2022, **628**, 122234.
29 L. Wang, J. Ma, J. Li, L. Fang and C. Liu, *Expert Opin. Drug Delivery*, 2025, 1–16.
30 D. M. Fitzgerald, Y. L. Colson and M. W. Grinstaff, *Prog. Polym. Sci.*, 2023, **142**, 101692.
31 S. Lobo, S. Sachdeva and T. Goswami, *Ther. Delivery*, 2016, **7**(1), 33–48.
32 C. Liu, P. Quan, S. Li, Y. Zhao and L. Fang, *J. Controlled Release*, 2017, **252**, 83–94.
33 C. Zhang, H. Luo, G. Lin, Z. Zhu, F. Zhang, J. Zhang, Y. Wu, J. Luo and H. Wang, *J. Drug Delivery Sci. Technol.*, 2016, **35**, 50–57.
34 M. K. Shukla, H. Tiwari, R. Verma, W. L. Dong, S. Azizov, B. Kumar, S. Pandey and D. Kumar, *Pharmaceutics*, 2023, **15**(2), 702.
35 A. M. Curreri, S. Mitragotri and E. E. L. Tanner, *Adv. Sci.*, 2021, **8**(17), e2004819.
36 K. Grodowska and A. Parczewski, *Acta Pol. Pharm.*, 2010, **67**, 3–12.
37 M. K. Ali, R. M. Moshikur, M. Goto and M. Moniruzzaman, *Pharmacal Res.*, 2022, **39**(10), 2335–2351.
38 S. H. Zeisel and K. A. da Costa, *Nutr. Rev.*, 2009, **67**(11), 615–623.
39 E. E. L. Tanner, A. M. Curreri, J. P. R. Balkaran, N. C. Selig-Wober, A. B. Yang, C. Kendig, M. P. Fluhr, N. Kim and S. Mitragotri, *Adv. Mater.*, 2019, **31**(27), e1901103.
40 E. E. L. Tanner, K. N. Ibsen and S. Mitragotri, *J. Controlled Release*, 2018, **286**, 137–144.
41 Y. Li, Q. Yu, Y. Lu, H. He, J. Qi, Z. Tai, Z. Chen, Q. Zhu and W. Wu, *Int. J. Pharm.*, 2024, **667**(Pt B), 125006.
42 L. R. Jorge, L. K. Harada, E. C. Silva, W. F. Campos, F. C. Moreli, G. Shimamoto, J. F. B. Pereira, O. J. Jr, M. Tubino, M. M. D. C. Vila and V. M. Balcão, *Front. Pharmacol.*, 2020, **11**, 243.
43 M. R. Islam, M. R. Chowdhury, R. Wakabayashi, Y. Tahara, N. Kamiya, M. Moniruzzaman and M. Goto, *Int. J. Pharm.*, 2020, **582**, 119335.
44 M. R. Islam, M. R. Chowdhury, R. Wakabayashi, N. Kamiya, M. Moniruzzaman and M. Goto, *Pharmaceutics*, 2020, **12**(4), 392.
45 M. Niemczak, D. K. Kaczmarek, T. Lejdysz, D. Gwiazdowska, K. Marchwińska and J. Pernak, *ACS Sustainable Chem. Eng.*, 2019, **7**(1), 1072–1084.
46 Y. Tahara, K. Morita, R. Wakabayashi, N. Kamiya and M. Goto, *Mol. Pharmaceutics*, 2020, **17**(10), 3845–3856.
47 M. K. Ali, R. M. Moshikur, R. Wakabayashi, Y. Tahara, M. Moniruzzaman, N. Kamiya and M. Goto, *J. Colloid Interface Sci.*, 2019, **551**, 72–80.
48 R. Islam, F. H. Nabila, R. Wakabayashi, N. Kamiya, M. Moniruzzaman and M. Goto, *J. Mol. Liq.*, 2024, **397**, 124184.
49 M. R. Islam, S. Uddin, M. R. Chowdhury, R. Wakabayashi, M. Moniruzzaman and M. Goto, *ACS Appl. Mater. Interfaces*, 2021, **13**(36), 42461–42472.
50 A. Bekdemir, E. E. L. Tanner, J. Kirkpatrick, A. P. Soleimany, S. Mitragotri and S. N. Bhatia, *Adv. Healthcare Mater.*, 2022, **11**(11), e2102685.
51 S. Zhang, C. Liu, Y. Song, J. Ruan, P. Quan and L. Fang, *J. Controlled Release*, 2023, **353**, 475–489.
52 Y. Sun, C. Liu, S. Ren, Y. Zhang, J. Ruan and L. Fang, *Eur. J. Pharm. Biopharm.*, 2023, **183**, 47–60.
53 S. Begum, H. Parvej, R. Dalui, S. Paul, S. Maity, N. Sepay, M. Afzal and U. C. Halder, *RSC Adv.*, 2023, **13**(48), 34097–34106.
54 S. N. Economidou, C. P. Pissinato Pere, M. Okereke and D. Douroumis, *Micromachines*, 2021, **12**(2), 117.
55 I. Brinkmann and C. C. Müller-Goymann, *Pharmazie*, 2005, **60**(3), 215–220.
56 C. Zhao, P. Quan, C. Liu, Q. Li and L. Fang, *Acta Pharm. Sin. B*, 2016, **6**(6), 623–628.
57 M. Parkash, M. H. Shoaib, M. Sikandar, R. I. Yousuf, M. T. Saleem, F. R. Ahmed and F. Siddiqui, *Sci. Rep.*, 2024, **14**(1), 28512.
58 M. S. Latif, F. F. Al-Harbi, A. Nawaz, S. A. Rashid, A. Farid, M. A. Mohaini, A. J. Alsalman, M. A. A. Hawaj and Y. N. Alhashem, *Polymers*, 2022, **14**(7), 1310.
59 N. G. Kotla, B. Chandrasekar, P. Rooney, G. Sivaraman, A. Larrañaga, K. V. Krishna, A. Pandit and Y. Rochev, *ACS Biomater. Sci. Eng.*, 2017, **3**(7), 1262–1272.
60 Y. Q. Yu, X. Yang, X. F. Wu and Y. B. Fan, *Front. Bioeng. Biotechnol.*, 2021, **9**, 646554.
61 A. Banerjee, K. Ibsen, Y. Iwao, M. Zakrewsky and S. Mitragotri, *Adv. Healthcare Mater.*, 2017, **6**(15), 1601411.
62 Q. M. Qi and S. Mitragotri, *J. Controlled Release*, 2019, **311–312**, 162–169.
63 T. Uchino, D. Kamiya, H. Yagi, H. Fujino-Shimaya, I. Hatta, S. Fujimori, Y. Miyazaki, Y. Kirishita, Y. Sano, H. Mizuno, K. Todoroki and Y. Kagawa, *Chem. Phys. Lipids*, 2023, **254**, 105305.
64 R. Mendelsohn, C. R. Flach and D. J. Moore, *Biochim. Biophys. Acta*, 2006, **1758**(7), 923–933.
65 S. Kozaka, Y. Tahara, R. Wakabayashi, T. Nakata, T. Ueda, N. Kamiya and M. Goto, *Mol. Pharmaceutics*, 2020, **17**(2), 645–655.
66 C. Wang, J. Zhu, D. Zhang, Y. Yang, L. Zheng, Y. Qu, X. Yang and X. Cui, *Int. J. Pharm.*, 2018, **535**(1–2), 120–131.
67 A. B. Nair, S. Gupta, A.-D. Be, S. Jacob, P. Shinu, J. Shah, M. A. Morsy, N. SreeHarsha, M. Attimarad, K. N. Venugopala and S. H. Akrawi, *Pharmaceutics*, 2019, **11**(7), 359.